

Study of hole concentration of 1,4-bis[N -(1-naphthyl)- N -phenylamino]- 4 , 4 diamine doped with tungsten oxide by admittance spectroscopy

Ming-Ta Hsieh, Chan-Ching Chang, Jenn-Fang Chen, and Chin H. Chen

Citation: *Applied Physics Letters* **89**, 103510 (2006); doi: 10.1063/1.2345610

View online: <http://dx.doi.org/10.1063/1.2345610>

View Table of Contents: <http://scitation.aip.org/content/aip/journal/apl/89/10?ver=pdfcov>

Published by the [AIP Publishing](#)

Articles you may be interested in

High response organic ultraviolet photodetector based on blend of 4 , 4 , 4 -tri-(2-methylphenyl phenylamino) triphenylamine and tris-(8-hydroxyquinoline) gallium

Appl. Phys. Lett. **93**, 103309 (2008); 10.1063/1.2980025

The origin of the hole injection improvements at indium tin oxide/molybdenum trioxide/ N , N -bis(1-naphthyl)- N , N -diphenyl- 1 , 1 -biphenyl- 4 , 4 -diamine interfaces

Appl. Phys. Lett. **93**, 043308 (2008); 10.1063/1.2965120

Interfacial electronic structure of N , N -bis(1-naphthyl)- N , N -diphenyl-1, 1 -biphenyl-4, 4 -diamine/copper phthalocyanine: C 60 composite/Au studied by ultraviolet photoemission spectroscopy

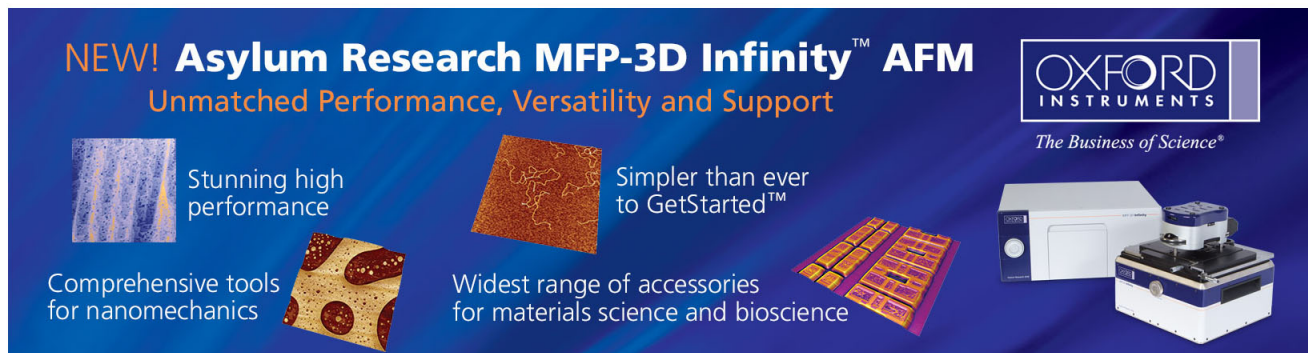
Appl. Phys. Lett. **91**, 052102 (2007); 10.1063/1.2761211

Pulsed-field ionization spectroscopy of high Rydberg states ($n = 50 - 200$) of bis(6 -benzene)chromium

J. Chem. Phys. **126**, 034308 (2007); 10.1063/1.2423022

Dielectric study on the flow alignment in 4- n -pentyl- 4 -cyanobiphenyl


J. Chem. Phys. **125**, 144517 (2006); 10.1063/1.2354154



NEW! Asylum Research MFP-3D Infinity™ AFM
Unmatched Performance, Versatility and Support

OXFORD INSTRUMENTS
The Business of Science®

Stunning high performance
Simpler than ever to GetStarted™
Comprehensive tools for nanomechanics
Widest range of accessories for materials science and bioscience



Study of hole concentration of 1,4-bis[*N*-(1-naphthyl)-*N'*-phenylamino]-4,4' diamine doped with tungsten oxide by admittance spectroscopy

Ming-Ta Hsieh,^{a)} Chan-Ching Chang, and Jenn-Fang Chen^{b)}

Department of Electrophysics, Nation Chiao Tung University, Hsinchu, Taiwan 30050, Republic of China

Chin H. Chen

Display Institute, MIRC, National Chiao Tung University, Taiwan 30050, Republic of China

(Received 23 January 2006; accepted 14 July 2006; published online 6 September 2006)

The effect of tungsten oxide (WO₃) incorporation into 1,4-bis[*N*-(1-naphthyl)-*N'*-phenylamino]-4,4' diamine (NPB) layer is investigated in NPB-tris(8-hydroxyquinoline)aluminium heterojunction organic light-emitting diodes. The admittance spectroscopy studies show that increasing the WO₃ volume percentage from 0% to 16% can increase the hole concentration of the NBP layer from 1.97×10^{14} to 1.90×10^{17} cm⁻³ and decrease the activation energy of the resistance of the NPB layer from 0.354 to 0.176 eV. Thus, this incorporation reduces the Ohmic loss and increases the band bending in the NBP layer near the interface, resulting in an improved hole injection via tunneling through a narrow depletion region. © 2006 American Institute of Physics. [DOI: 10.1063/1.2345610]

Since Tang and VanSlyke fabricated the first organic light emitting diodes (OLEDs),¹ the applications of OLEDs have attracted considerable attention. However, the low power efficiency and high driving voltage limit their further development. In order to obtain high efficiency, many methods have been developed to improve the carrier injection from the electrode to the transporting layer.²⁻⁷ Despite these efforts, the operating voltage is still not low enough for display applications. Recently, doping the transport layer for enhancing carrier injection and lowering drive voltages has been demonstrated. Electrical doping of molecular films by insertion of electron accepting (*p* dopants) atoms or molecules has been shown to increase the film conductivity.⁸⁻¹⁰ So far, the most widely investigated *p* dopants for organic films are tetracyanoquinodimethane (TCNQ) and its fluorinated derivative tetrafluorotetracyanoquinodimethane (F4-TCNQ).¹¹⁻¹⁴ However, using highly volatile F4-TCNQ in thermal evaporation under high vacuum has raised serious concerns over issues of cross contamination, chamber pollution, and the thermal stability. In our previous work, we used tungsten oxide (WO₃) as a *p* dopant which exhibits good electric properties.¹⁵ In this letter, we continue to study the effect of the WO₃ incorporation into the 1,4-bis[*N*-(1-naphthyl)-*N'*-phenylamino]-4,4' diamine (NPB) layer on the electrical characteristics of NPB-tris(8-hydroxyquinoline)aluminium (Alq₃) heterojunction organic light-emitting diodes by performing admittance spectroscopy.

The studied structure is indium-tin-oxide (ITO)/NPB:WO₃ (0%–33%) (60 nm)/Alq₃ (60 nm)/aluminum (Al). Doped layers (NPB:WO₃) were prepared by coevaporation of NPB as the matrix and WO₃ as a dopant. In the doped layers, the WO₃ volume percentages are 0%, 9%, 16%, and 33%. The structures thus formed are referred to as devices A, B, C, and D, respectively. The organic materials were deposited on an ITO-coated glass by thermal evapora-

tion in an ULVAC Solciet OLED coater at a base vacuum pressure of 10⁻⁷ Torr and at a growth rate of 1 Å/s. The thickness and sheet resistance of the ITO layer were 100 nm and 35 Ω/sq. The Al metal cathode was prepared by thermal vapor deposition at 10⁻⁶ Torr and at the rate of 5 Å/s. Before depositing the organic materials, the ITO-coated glass was cleaned in acetone, isopropyl alcohol, and de-ionized water and then was treated with oxygen plasma for 30 s. The device was hermetically sealed prior to measurement in nitrogen ambient. The active area was 3 × 3 mm² which was defined by the overlap of the ITO and the cathode electrode. Admittance spectroscopy was performed to obtain the equivalent circuit of the device by using an HP4194A gain phase analyzer with an oscillation level of 0.1 V.

Figure 1 shows the 300 K capacitance-frequency (*C-F*) and conductance/frequency-frequency (*G/F-F*) spectra, measured at zero bias on device A. The spectra show two capacitance drops and *G/F* peaks at inflexion frequencies around 25 kHz and 0.42 MHz, suggesting the presence of two geometric resistance-capacitance (*RC*) time constant effects. Based on these spectra, an equivalent circuit model as shown is developed, where *C*₁, *R*₁ and *C*₂, *R*₂ represent the

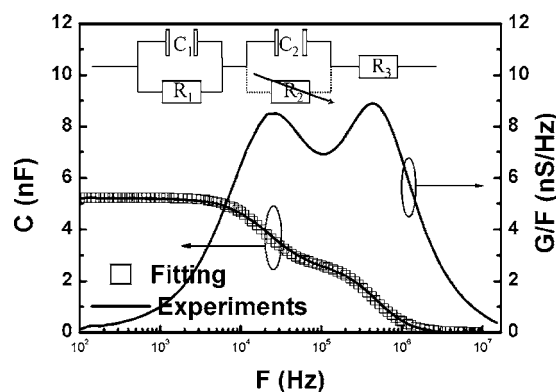


FIG. 1. Spectra of the admittance spectroscopy, measured on a heterojunction device with an ITO/NPB(60 nm)/Alq₃(60 nm)/Al structure. The *C-F* spectra agree with simulated spectra (open squares) based on an equivalent circuit model using *C*₁=5.40 nF, *C*₂=5.23 nF, *R*₁=3.9 kΩ, and *R*₃=850 Ω.

^{a)} Author to whom correspondence should be addressed; electronic mail: mthsieh.ep94g@nctu.edu.tw

^{b)} Electronic mail: jfchen@cc.nctu.edu.tw

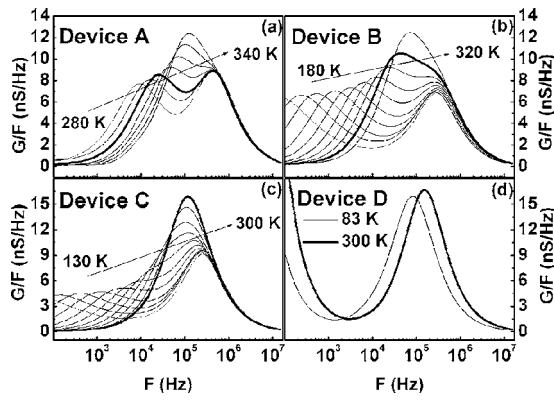


FIG. 2. Temperature-dependent G/F - F spectra at zero bias for devices (a) A, (b) B, (c) C, and (d) D. The rapid increase at low frequency in (d) is due to leakage current.

geometric capacitance and resistance of the NPB layer and the Alq_3 layer, respectively, and R_3 represents the series resistance which can be ascribed to parasitic effects due to lead/contact resistances.¹⁶ In these studied devices, R_2 can be treated as an open circuit because it is much larger than R_1 and R_3 . Based on this equivalent circuit, the total equivalent capacitance is given by

$$C(\omega) = \frac{C_0}{1 + (C_0^2 R_3^2 \omega^2)}, \quad (1)$$

where C_0 is

$$C_0 = \frac{C_1 C_2}{C_1 + C_2} \left[1 + \frac{C_2 / C_1}{1 + \omega^2 R_1^2 (C_1 + C_2)^2} \right]. \quad (2)$$

Details of the theory on admittance spectroscopy can be found elsewhere.^{17,18} Excellent agreement is found between the experimental (solid curve) and simulated (open squares) C - F spectra by selecting $C_1 = 5.40$ nF, $C_2 = 5.23$ nF, $R_3 = 850 \Omega$, and $R_1 = 3.9$ k Ω (Notably, if $R_1 < R_3$, the spectra exhibit only one steplike capacitance drop). The capacitance below ~ 1 kHz is C_2 whose value (5.26 nF) is comparable to a value of 5.31 nF determined from the thickness of the Alq_3 layer according to a parallel-capacitor model $C = \epsilon_r \epsilon_0 A / d$ (with $\epsilon_r \sim 4$).¹⁹ As frequency increases, the carriers charging the NPB layer cannot follow ac probing frequency and the capacitance drops at the inflexion frequency of ~ 25 kHz which equals to the inverse of the RC time constant of the NPB layer by the relationship $\omega_{\text{inflexion}} = \tau^{-1} = [R_1(C_1 + C_2)]^{-1}$. When frequency is increased beyond this inflexion frequency, the capacitance reaches a plateau whose value is the series combination of C_1 and C_2 . Therefore, values of C_1 , C_2 , and R_1 can be determined. When frequency further increases, the capacitance drops again due to the series resistance R_3 . Note that the two inflexion frequencies can be more clearly seen in the G/F peaks.

Figure 2 shows the temperature-dependent G/F - F spectra of the studied devices, measured at zero bias. In devices A–C, the spectra show two distinct peaks: the low-frequency peak is associated with the resistance of the NPB layer and high-frequency peak is associated with the parasitic series resistance. While the series-resistance peak does not depend on temperature the NPB peak displays significant temperature dependence. For comparison, the spectrum measured at 300 K is boldfaced. As the WO_3 volume percentage increases, the NPB peak shifts gradually toward high fre-

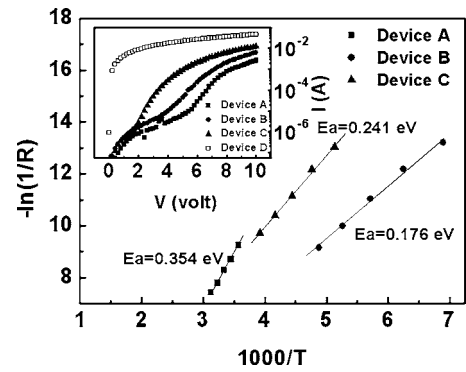


FIG. 3. Plots of $-\ln(1/R_{\text{NPB}})$ vs $1000/T$. The resistance R_{NPB} is derived from the low-frequency peak in the G/F - F spectra in Fig. 2. The room-temperature I - V curves of the studied devices are shown in the inset.

quency and finally mixes with the series-resistance peak, indicating a decrease of the resistance of the NPB layer. As temperature decreases, the NPB peak shifts toward low frequency. This temperature dependence becomes less pronounced as the WO_3 volume percentage increases, suggesting a decrease in the activation energy. In general, the resistance of the NPB layer can be expressed by a simple geometric equation,

$$R_{\text{NPB}} = \frac{L}{q \mu_{\text{NPB}} N_{\text{HOMO}} \exp(-E_a/kT) A}, \quad (3)$$

where q is the electron charge, μ_{NPB} the mobility of the NPB layer, N_{HOMO} the density of states function in the highest occupied molecular orbital (HOMO), E_a the activation energy, A the area, and L the thickness of the NPB layer. The obtained values of R_{NPB} and its activation energy are shown in plots of $-\ln(1/R_{\text{NPB}})$ vs $1000/T$ in Fig. 3. As shown, increasing the WO_3 volume percentage from 0% to 9% and then to 16% reduces the activation energy from 0.354 to 0.241 and then to 0.176 eV.

From R_{NPB} and E_a of device A, using $\mu_{\text{NPB}} = 5.1 \times 10^{-4}$ $\text{cm}^2/\text{V s}$ obtained from Chen *et al.*,²⁰ the value of N_{HOMO} is determined to be 1.698×10^{20} cm^{-3} . From this value, the mobilities for the devices B–D are determined and the results are summarized in Table I. Increasing the WO_3 volume percentage from 0% to 16% reduces the resistance of the NPB layer from 3.89×10^3 to $4.03 \times 10^2 \Omega$ due to an increase in the hole concentration from 1.97×10^{14} to 1.90×10^{17} cm^{-3} and a decrease of mobility from 5.1×10^{-4} to 5.1×10^{-6} $\text{cm}^2/\text{V s}$. When the WO_3 volume percentage further increases to 33%, as indicated in Fig. 2(d), the NPB peak cannot be resolved from the series-resistance peak, and thus the exact resistance of the NPB layer cannot be obtained but, judging from its likely position,

TABLE I. Electric parameters derived from experimental measurements at room temperature.

Device (WO_3 %)	Hole concentration (cm^{-3})	Mobility ($\text{cm}^2/\text{V s}$)	Resistance (Ω)
Device A (0%)	1.97×10^{14}	5.10×10^{-4}	3.89×10^3
Device B (9%)	1.54×10^{15}	7.71×10^{-5}	9.86×10^2
Device C (16%)	1.90×10^{17}	5.10×10^{-6}	4.03×10^2
Device D (33%)	$> 10^{17}$	$< 10^{-6}$	$< 10^2$

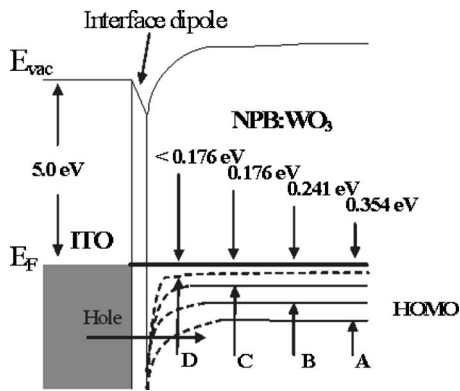


FIG. 4. Schematic diagram of the device band structure, showing a decrease in the energy separation between the edge of the HOMO and Fermi level in the bulk of the NPB layer due to the WO_3 incorporation.

it must be less than $10^2 \Omega$. The rapid increase at low frequency in Fig. 2(d) reflects the leakage current due to negligible energy barrier, as will be shown later.

Figure 4 shows the schematic band diagram of the device with an energy barrier in the HOMO between the ITO and NPB. Since the activation energy represents the energy separation between the edge of the HOMO and Fermi level, the WO_3 incorporation decreases this energy separation in the bulk of the NPB layer. As a result, the width of the energy barrier is reduced and the hole injection from the ITO to NPB layer is improved via tunneling through a narrow depletion region. This enhanced tunneling causes current conduction at small voltages, as shown in the inset of Fig. 3, where the room-temperature current-voltage (I - V) characteristics of the studied devices are shown. The current conduction is enhanced from device A to C due to a reduced energy barrier and, in device D, the current conduction is nearly Ohmic due to a negligible energy barrier. The negligible energy barrier causes the nearly Ohmic conduction, which can explain the leakage current at small voltage in device D. This result also demonstrates that the current conduction is mainly

governed by the hole injection from the ITO anode to the NPB layer.

The authors would like to thank the National Science Council of the Republic of China, Taiwan for financially supporting this research under Contract No. 94-2112-M-009-029 and MOE ATU Program. This work is partially supported by Chunghwa Picture Tubes Ltd.

- ¹C. W. Tang and S. A. Vanslyke, *Appl. Phys. Lett.* **51**, 913 (1987).
- ²J. S. Kim, M. Granstrom, R. H. Friend, N. Johansson, W. R. Salaneck, R. Daik, W. J. Feast, and F. Cacialli, *J. Appl. Phys.* **84**, 6859 (1998).
- ³M. G. Mason, L. S. Hung, C. W. Tang, S. T. Lee, K. W. Wong, and M. Wang, *J. Appl. Phys.* **86**, 1688 (1999).
- ⁴S. A. VanSlyke, C. H. Chen, and C. W. Tang, *Appl. Phys. Lett.* **69**, 2160 (1996).
- ⁵Y. Yang and A. H. Heeger, *Appl. Phys. Lett.* **64**, 1245 (1994).
- ⁶T. Grandlund, L. A. A. Pettersson, and O. Inganäs, *J. Appl. Phys.* **89**, 5897 (2001).
- ⁷Y. Shirota, Y. Kuwabara, D. Okuda, R. Okuda, H. Ogawa, H. Inada, T. Wakimoto, H. Nakada, Y. Yonemoto, S. Kawami, and K. Imai, *J. Lumin.* **72-74**, 985 (1997).
- ⁸C. Ganzorig and M. Fujihira, *Appl. Phys. Lett.* **77**, 4211 (2000).
- ⁹A. Yamamori, C. Adachi, T. Koyama, and Y. Taniguchi, *Appl. Phys. Lett.* **72**, 2147 (1998).
- ¹⁰J. Endio, T. Matsumoto, and J. Kido, *Jpn. J. Appl. Phys., Part 2* **41**, L358 (2002).
- ¹¹J. Blochwitz, M. Pfeiffer, T. Fritz, and K. Leo, *Appl. Phys. Lett.* **73**, 729 (1998).
- ¹²M. Pfeiffer, T. Fritz, J. Blochwitz, A. Nollau, B. Plonnigs, A. Beyer, and K. Leo, *Adv. Solid State Phys.* **39**, 77 (1999).
- ¹³M. Pfeiffer, A. Beyer, T. Fritz, and K. Leo, *Appl. Phys. Lett.* **73**, 3202 (1998).
- ¹⁴J. Blochwitz, M. Pfeiffer, T. Fritz, K. Leo, D. M. Alloway, P. A. Lee, and N. R. Armstrong, *Org. Electron.* **2**, 97 (2001).
- ¹⁵C. C. Chang, M. T. Hsieh, J. F. Chen, S. W. Hwang, J. W. Ma, and C. H. Chen, *SID'06 Digest XXXVII*, 1106 (2006).
- ¹⁶W. Brütting, H. Riel, T. Beierlein, and W. Riess, *J. Appl. Phys.* **89**, 1704 (1994).
- ¹⁷W. G. Oldham and S. S. Naik, *Solid-State Electron.* **15**, 1085 (1972).
- ¹⁸S. W. Tsang, S. K. So, and J. B. Xu, *J. Appl. Phys.* **99**, 013706 (2006).
- ¹⁹Stefan Berleb and Wolfgang Brütting, *Phys. Rev. Lett.* **89**, 286601 (2002).
- ²⁰B. Chen, C. S. Lee, S. T. Lee, P. Webb, Y. C. Chan, W. Gambling, H. Tian, and W. Zhu, *Jpn. J. Appl. Phys., Part 1* **39**, 1190 (2000).